



Quasi-two-dimensional anisotropic superconductivity in Li-intercalated 2H-TaS₂T. Agarwal, C. Patra, A. Kataria , Rajeswari R. Chowdhury, and R. P. Singh **Department of Physics, Indian Institute of Science Education and Research Bhopal, Bhopal 462066, India*

(Received 9 March 2023; revised 22 April 2023; accepted 25 April 2023; published 8 May 2023)

Two-dimensional (2D) superconductivity in artificial interfaces and atomic-thin layers has gained attention for its exotic quantum phenomena and practical applications. Although bulk van der Waals layered materials have been explored for 2D superconductivity, most of these compounds do not exhibit remarkable properties despite exhibiting 2D characteristics. Here we report a comprehensive analysis of single crystals of Li-intercalated 2H-TaS₂ superconductor, suggesting weakly coupled anisotropic superconductivity. Angle-dependent magnetotransport and the Berezinskii-Kosterlitz-Thouless transition confirm quasi-2D superconductivity in 2H-Li_xTaS₂.

DOI: [10.1103/PhysRevB.107.174509](https://doi.org/10.1103/PhysRevB.107.174509)**I. INTRODUCTION**

Recent studies on superconductivity in reduced dimension have drawn increasing attention to exploring new phenomena such as quantum metallic ground state, quantum Griffith singularity, and Ising superconductivity [1–5]. Superconductivity in two-dimensional materials has been observed in materials where their thickness is less than the superconducting coherence length ($d < \xi$), such as in thin films and heterostructured interfaces [6–8]. However, achieving superconductivity in materials with an atomic limit thickness, where it is susceptible to disorders, poses a significant challenge. Anisotropic layered materials, such as MoS₂, NbSe₂, and ZrNCl, offer a promising platform to study two-dimensional (2D) superconductivity and have exhibited unconventional properties [9,10]. Recently, clean limit 2D superconductivity has been discovered in bulk Ba₆Nb₁₁S₂₈ due to the presence of sublayers NbS₂ and Ba₃NbS₅ [11].

Layered transition metal dichalcogenides (TMDs) have attracted particular interest due to their broad range of properties, including dimension-dependent band structure, polymorphic phase transitions, and significant electron-electron and electron-phonon interactions [12–14]. These systems exhibit novel phenomena, such as the coexistence of charge density wave (CDW) and superconductivity, metal-insulator transition, spin-valley coupling, and quantum spin Hall effect, due to their 2D nature and the strong spin-orbit coupling effect caused by heavy metal atoms [15–17]. Moreover, TMDs in the few-layer limit exhibit extremely high in-plane upper critical field (H_{c2}) values that exceed the Pauli limiting field several times, which can be attributed to their inherent strong spin-orbit coupling and inversion symmetry breaking, leading to exotic forms of superconductivity [5,18]. However, the fabrication processes for low-dimensional materials are typically complicated, and this may hinder their characterization through various techniques, which is essential for a complete understanding of the phenomena. Intercalation or chemical doping of these materials represents an alternate

way to achieve 2D superconductivity by modifying interlayer coupling and electronic properties. Reports have shown that quasi-2D superconductivity can be achieved by adjusting the interlayer coupling in materials such as AuTe₂Se_{4/3}, organic-ion-intercalated SnSe₂, and Pb_{1/3}TaS₂ [19–21].

TaS₂ is an important member of the TMD family, with various polytypes determined by the arrangement of Ta and S atoms, exhibiting unique and fascinating properties. The 2H-TaS₂ family displays chiral charge ordering [22] while substituting S atoms with Se atoms in 2H-TaSeS leads to 2D multigap superconductivity that breaks the Pauli limit [23]. Furthermore, intercalated 2H-TaS₂ with organic molecules like (Py)_{0.5}TaS₂, where Py represents pyridine, has shown a dimensional crossover from 3D to 2D [24].

In this paper, we have reported single-crystal growth and superconducting properties of the Li-intercalated 2H-TaS₂ compound using transport, magnetization, and specific heat measurements. It confirms weakly coupled anisotropic superconductivity having bulk superconducting transition at $T_c = 3.3(1)$ K. Detailed specific heat measurement identifies Li_xTaS₂ as a weakly coupled superconductor. Angle-dependent magnetotransport and Berezinskii-Kosterlitz-Thouless (BKT) transition ($T_{BKT} = 2.9$ K) confirm the quasi-2D superconductivity in 2H-Li_xTaS₂.

II. EXPERIMENTAL DETAILS

Single crystals of the Li_xTaS₂ compound were synthesized using the chemical vapor transport (CVT) method. The starting materials Ta powder (99.9%) and S powder (99.5%) were used in the required ratio with LiCl as a transporting agent. Li_xTaS₂ was prepared with a Li content of 0.3 in LiCl. The powder was sealed in a quartz tube after the tube was evacuated to $\sim 10^{-6}$ mbar. The sealed tube was placed in a two-zone tubular furnace and heated at a temperature gradient of 1083–1053 K for 10 days and then slowly cooled to room temperature. Shiny millimeter-sized crystals were obtained in the cold zone.

Powder x-ray diffraction (XRD) measurements were performed on a single-crystalline sample and crushed crystals using an X'pert PANalytical diffractometer with monochromatic

*rpsingh@iiserb.ac.in

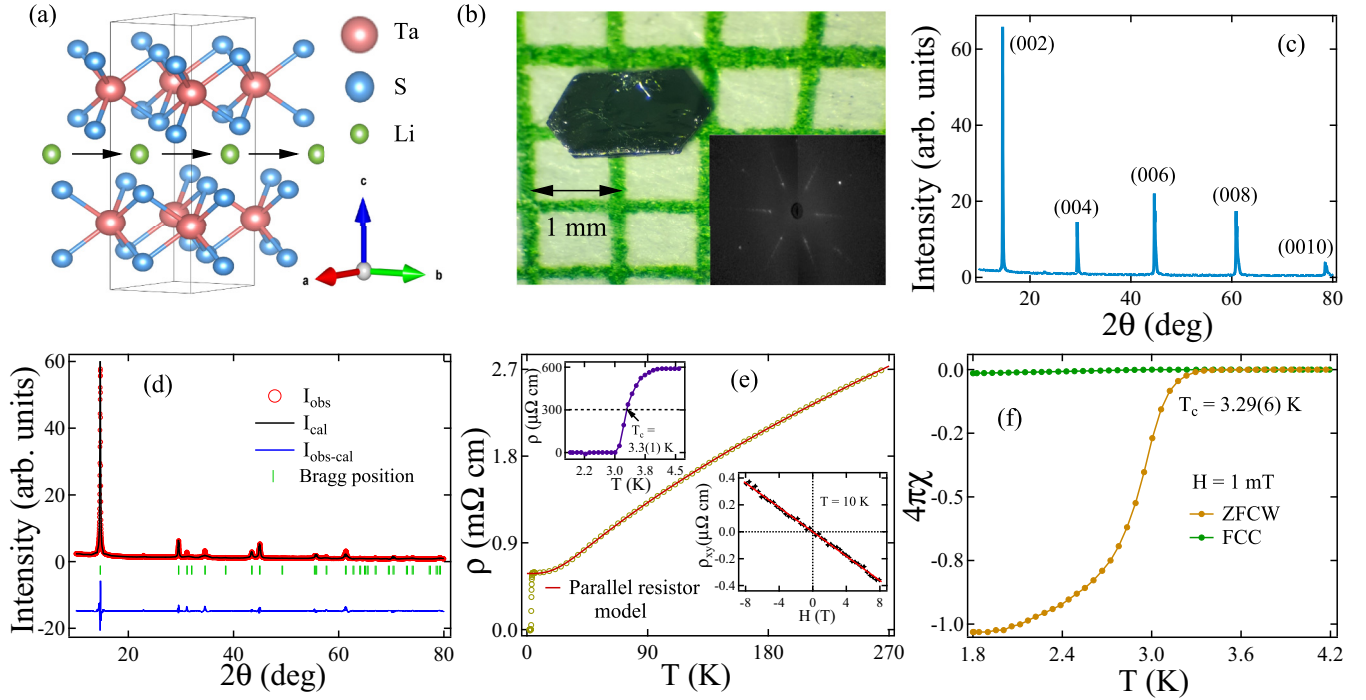


FIG. 1. (a) The crystal structure of Li-intercalated $2H$ - TaS_2 . (b) The single-crystal image of Li-intercalated $2H$ - TaS_2 , and the inset shows the Laue diffraction pattern of the crystal. (c) Single-crystal XRD with labeled $[00l]$ reflections which indicates the c axis as the growth direction. (d) Powder XRD of well-crushed crystals refined with a $2H$ - TaS_2 hexagonal structure. (e) Temperature-dependent electrical resistivity at zero field fitted with the parallel resistor model. The inset (upper left) shows a zoomed view of the zero drop transition of resistivity in the superconducting region. The lower inset shows the Hall resistivity at $T = 10$ K with a negative slope, indicating n -type charge carriers in Li_xTaS_2 . (f) Temperature dependence of magnetic susceptibility in both the ZFCW and FCC modes measured at $H = 1$ mT in the $H \perp c$ direction.

Cu $K\alpha$ radiation ($\lambda = 1.5406$ Å) to determine the structure and phase purity of the sample. The Laue diffraction pattern was recorded using a Photonic-Science Laue camera system. A Quantum Design magnetic measurement system (MPMS3) was used to measure magnetization. Transport and specific heat measurements were also conducted using a Quantum Design physical property measurement system. A Quantum Design horizontal rotator insert was used for angle-dependent magnetotransport measurements, and all transport data were collected using the standard four-probe method.

III. RESULTS AND DISCUSSION

A. Sample characterization

Figure 1(a) shows the crystal structure of $2H$ - TaS_2 where Li is intercalated within the layers. In the $2H$ phase, the Ta atom is coordinated in a trigonal prismatic pattern with chalcogen S atoms. Figure 1(b) shows the crystal image obtained by the CVT method with a Laue pattern in the inset. The single-crystal XRD pattern of Li_xTaS_2 is shown in Fig. 1(c), reflecting crystal growth in the c direction with $[00l]$ peaks. Powder XRD was performed on well-crushed crystals. The observed, calculated, and difference Rietveld profiles for powdered Li_xTaS_2 have been shown in Fig. 1(d) with Bragg positions. To deduce the lattice parameters, we performed XRD refinement using FULLPROF software. Li_xTaS_2 has a hexagonal structure similar to the parent compound TaS_2 with the $P6_3/mmc$ (194) space group. The obtained lattice

parameters are $a = b = 3.315(6)$ Å, $c = 12.093(3)$ Å where a slight increase in the c parameter is observed as compared to $2H$ - TaS_2 [25]. However, no significant changes in the lattice parameters indicate that Li atoms have intercalated between the weakly bonded layers instead of residing at atomic sites.

B. Anisotropic superconductivity

Figure 1(e) presents the zero-field resistivity variation with temperature. As the resistivity decreased with decreasing temperature from 300 to 10 K, it indicated metallic conduction in the normal state. The residual resistivity ratio [RRR = $\rho(300 \text{ K})/\rho(6 \text{ K})$] is obtained as 4.6. In the zero field, an abrupt drop in resistivity is observed at $T_c = 3.3(1)$ K, indicating the occurrence of superconductivity in this compound. The inset of Fig. 1(e) (upper left) shows the enlarged view of the resistivity around the superconducting region. A similar superconducting transition has been reported earlier in Li_xTaS_2 with $x = 0.096$ [26]. As in the normal-state resistivity, no change of curvature or any kink was spotted, which is attributed to the suppression of CDW transition by Li intercalation, whereas in parent $2H$ - TaS_2 a CDW anomaly has been reported at $T_{\text{CDW}} \sim 75$ K [27]. Normal-state resistivity is well fitted by the parallel resistor model, according to which temperature-dependent resistivity is given by

$$\rho(T) = \left[\frac{1}{\rho_{\text{sat}}} + \frac{1}{\rho_{\text{ideal}}(T)} \right]^{-1}, \quad (1)$$

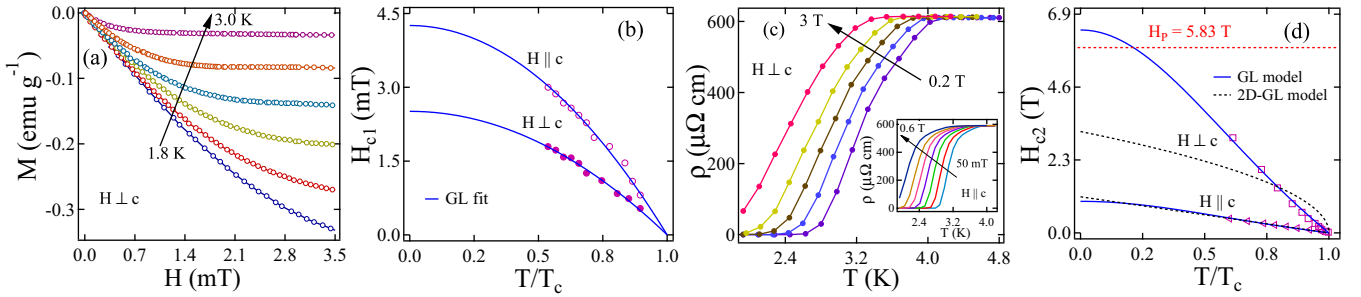


FIG. 2. (a) Field-dependent magnetization plot to calculate lower critical field value. (b) Temperature dependence of the lower critical field values in both directions. The solid blue line shows the GL-fitted curve. (c) Low-temperature resistivity at different fields in the $H \perp c$ direction where broad transition indicates effective vortex dynamics in the superconducting region. Inset shows the temperature dependence of resistivity in the $H \parallel c$ direction. (d) Temperature dependence of the upper critical field in both directions manifests anisotropy in the superconductivity. The blue and black lines are fitted to the GL model and the 2D GL model, respectively. The red dotted line indicates the Pauli limiting field.

where ρ_{sat} is the saturated resistivity at high temperature, which is temperature independent, and $\rho_{\text{ideal}}(T)$ can be written as $\rho_{\text{ideal}}(T) = \rho_0 + \rho_{i,L}(T)$. Here ρ_0 is the temperature-independent residual resistivity arising from impurity scattering, and $\rho_{i,L}(T)$ can be defined by Wilson's theory as [28]

$$\rho_{i,L}(T) = C \left(\frac{T}{\theta_D} \right)^r \int_0^{\theta_D/T} \frac{x^r}{(e^x - 1)(1 - e^{-x})} dx. \quad (2)$$

Here θ_D denotes Debye temperature, and C is the material-dependent constant. After fitting with $r = 3$, the residual resistivity values $\rho_0 = 0.611(2)$ m Ω cm and the Debye temperature $\theta_D = 165(2)$ K are extracted.

To calculate the carrier density of Li_xTaS_2 , Hall measurement was performed. The Hall resistivity ρ_{xy} follows a general linear behavior with varying magnetic field, and the slope value gives the Hall coefficient (R_H) as shown in the lower right inset of Fig. 1(e). By linear fit, we obtained $R_H = 4.59 \times 10^{-12}$ cm³ C⁻¹ and accordingly the carrier density $n = 1.36 \times 10^{22}$ cm⁻³ using the formula $R_H = 1/ne$. The negative slope indicates that electrons are the dominant charge carriers in the system.

To determine the superconducting transition temperature, magnetic susceptibility was measured under an applied field of 1 mT. Figure 1(f) displays the temperature dependence of the magnetic susceptibility in both the zero-field-cooled warming (ZFCW) and field-cooled cooling (FCC) modes in the $H \perp c$ direction. Below the critical temperature of $T_c = 3.29(6)$ K, a significant diamagnetic signal was observed, indicating the onset of the superconducting state. The FCC signal was weaker than the ZFCW signal due to strong flux trapping in the sample. According to the ZFCW data, the superconducting volume fraction was estimated to be $\sim 100\%$, which confirms the bulk superconductivity in Li_xTaS_2 .

Magnetization-field (M - H) data were collected at various temperatures to determine the lower critical field value, H_{c1} , as presented in Fig. 2(a). The H_{c1} values at a particular temperature were extracted from where the M - H curve deviates from the linear Meissner effect ($M = -H$). $H_{c1}(0)$ was estimated by fitting the data as a function of temperature, using the Ginzburg-Landau (GL) relation given in Eq. (3). The $H_{c1}(0)$ value was obtained from the fit intercept, as shown in Fig. 2(b)

for both directions [29].

$$H_{c1}(T) = H_{c1}(0) \left[1 - \left(\frac{T}{T_c} \right)^2 \right]. \quad (3)$$

The fitting results indicated that the zero-temperature values $H_{c1}^{\parallel}(0)$ (parallel to the c axis) and $H_{c1}^{\perp}(0)$ (perpendicular to the c axis) were 4.25 (4) and 2.51 (2) mT, respectively.

The upper critical field value H_{c2} was determined by measuring the temperature dependence of the resistivity under various magnetic fields for both orientations as $H \parallel c$ and $H \perp c$ as presented in Fig. 2(c). The values of H_{c2} were obtained by setting $\rho = 0.1\rho_n$, where ρ_n represents the resistivity in the normal state. The resulting H_{c2} values as a function of temperature are shown in Fig. 2(d). Data were fitted using GL and 2D GL models. For perfect 2D superconductors, H_{c2}^{\perp} follows a $(1 - T/T_c)^{1/2}$ behavior in the $H \perp c$ direction. However, the H_{c2} data obtained in the $H \perp c$ direction deviates from the 2D GL model and is well described by the GL model. According to the GL model, H_{c2} follows:

$$H_{c2}(T) = H_{c2}(0) \left[\frac{1 - \left(\frac{T}{T_c} \right)^2}{1 + \left(\frac{T}{T_c} \right)^2} \right]. \quad (4)$$

The H_{c2} data in the $H \parallel c$ direction are consistent with both models. Based on the GL model, the estimated values of $H_{c2}^{\parallel}(0)$ and $H_{c2}^{\perp}(0)$ are 0.99(2) and 6.40(3) T, respectively. The deviation from the 2D GL model indicates that the superconducting TaS_2 layers are not fully decoupled, suggesting quasi-2D superconductivity in Li_xTaS_2 .

The obtained anisotropic parameter [$\Gamma = H_{c2}^{\perp}(0)/H_{c2}^{\parallel}(0)$] of 6.5, which is slightly lower than that of the parent $2H$ - TaS_2 [30]. $\text{Na}_{0.1}\text{TaS}_2$, $\text{Cu}_{0.03}\text{TaS}_2$, and $\text{Ni}_{0.04}\text{TaS}_2$ also show similar anisotropy [31–33], which can be attributed to the anisotropy of the Fermi surface. In 2D superconductors, Cooper pairing can be disrupted primarily by the Pauli paramagnetic mechanism, as the orbital effect is negligible due to the constrained electron dynamics in a plane. The Pauli paramagnetic limit, also called the Clogston-Chandrasekhar limit, is given by the equation $H_p = 1.86$ (T K⁻¹) T_c . In the case of Li_xTaS_2 , the Pauli limit is $H_p = 5.83$ T (with $T_c = 3.12$ K at $\rho = 0.1\rho_n$), which is below the in-plane upper critical field value [$H_{c2}^{\perp}(0)$] and indicates a violation

TABLE I. The anisotropic superconducting parameters of Li_xTaS_2 single crystal.

Parameters	Unit	$H \parallel c$	$H \perp c$
$H_{c1}(0)$	mT	4.25(4)	2.51(2)
$H_{c2}(0)$	T	0.99(2)	6.40(3)
ξ	nm	2.82(8)	18.20(8)
λ_{GL}	nm	838.21(8)	336.02(2)
k_{GL}		18.5	74.1

of the Pauli limit. Possible reasons for this deviation in 2D superconductors include Ising spin-orbit coupling (SOC), Fulde-Ferrell-Larkin-Ovchinnikov (FFLO) states, and spin-orbit scattering [34–36]. However, further theoretical analysis is necessary to determine the underlying cause of the Pauli limit breaking in Li_xTaS_2 .

For anisotropic superconductors, the relation between the upper critical field and the coherence length (ξ) can be expressed by Eq. (5) as

$$H_{c2} = \frac{\phi_0}{2\pi\xi_{\perp}^2} (\cos^2\theta + \epsilon^2 \sin^2\theta)^{-1/2}. \quad (5)$$

Here, ϕ_0 is the magnetic flux quanta with a value of $2.07 \times 10^{-15} \text{ T m}^2$, θ denotes the angle between the applied field and the unit vector perpendicular to the layers, and ϵ is the ratio of the two coherence lengths, i.e., $\epsilon = \xi_{\parallel c}/\xi_{\perp c}$. We can obtain the expressions for the coherence length along the parallel ($\xi_{\parallel c}$) and perpendicular ($\xi_{\perp c}$) directions to the c axis by reducing Eq. (5) for $\theta = 0^\circ$ and 90° , which are given by $H_{c2}^{\parallel}(0) = \frac{\phi_0}{2\pi\xi_{\parallel}^2}$ and $H_{c2}^{\perp}(0) = \frac{\phi_0}{2\pi\xi_{\perp}^2}$, respectively. The values of $\xi_{\parallel c}$ and $\xi_{\perp c}$ were determined to be 2.82(8) and 18.20(8) nm, respectively.

The GL penetration length and the GL parameter κ were calculated using the equations $H_{c2}^{\perp}(0)/H_{c1}^{\perp}(0) = 2\kappa_{\perp}^2/\ln\kappa_{\perp c}$, $\kappa_{\perp c} = [\lambda_{\perp c}(0)\lambda_{\parallel c}(0)/\xi_{\perp c}(0)\xi_{\parallel c}(0)]^{1/2}$, and $\kappa_{\parallel c} = \lambda_{\perp c}(0)/\xi_{\perp c}(0)$. All the obtained superconducting parameters are summarized in Table I. The value of $\kappa > 1/\sqrt{2}$ indicates that Li_xTaS_2 is an extreme type-II superconductor. The critical thermodynamic field, which is a measure of condensation energy, was estimated to be approximately 0.06 T using $H_c(0) = H_{c1}^{\perp}(0)\sqrt{2\kappa_{\perp c}/\ln\kappa_{\perp c}}$.

The anisotropy ratios for different intercalating atoms in the $2H\text{-TaS}_2$ phase are listed in Table II to compare the anisotropy of Li_xTaS_2 . Furthermore, the mean free path (l_e) was calculated using the Drude model, $l_e = (3\pi^2)^{1/3}\hbar/e^2\rho_0n^{2/3}$, where ρ_0 is the residual resistivity and

TABLE II. Comparison of the anisotropy ratio of Li_xTaS_2 with different intercalated $2H\text{-TaS}_2$ compounds.

Compounds	T_c (K)	H_{c2}^{\parallel} (T)	H_{c2}^{\perp} (T)	Γ
Li_xTaS_2	3.3	0.99	6.40	6.5
$\text{Na}_{0.1}\text{TaS}_2$ [31]	4.3	2.5	16	6.4
$\text{Ni}_{0.04}\text{TaS}_2$ [33]	4.15	4.85	17.3	3.58
$\text{Cu}_{0.03}\text{TaS}_2$ [32]	4.03	1.8	9.16	5.1
$\text{Pb}_{0.03}\text{TaS}_2$ [21]	2.8	0.4	6.84	17.1
$\text{In}_{0.58}\text{TaS}_2$ [37]	0.69	0.028	0.34	12

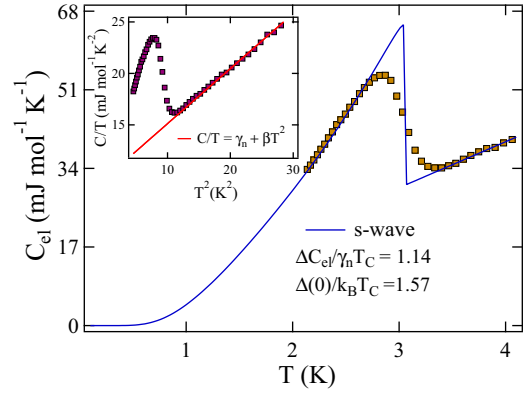


FIG. 3. The electronic contribution to the specific heat is plotted as a function of T . The solid blue line displays a BCS type behavior. Inset shows the temperature dependence of specific heat where the jump at $T_c \sim 3.33(6)$ K depicts a phase transition from the normal to the superconducting state.

n is the carrier concentration. The calculated value of l_e was 0.366 nm using the values of $\rho_0 = 0.611(2) \text{ m}\Omega \text{ cm}$ and $n = 1.36 \times 10^{22} \text{ cm}^{-3}$. Since $l_e/\xi_0 = 0.0201 \ll 1$, it indicates that Li_xTaS_2 is a dirty limit superconductor.

C. Specific heat measurement

The presence of superconductivity in Li_xTaS_2 is confirmed by the discontinuity in the zero-field specific heat at $\sim 3.33(6)$ K, shown in the inset of Fig. 3. The total specific heat is expressed as $\frac{C}{T} = \gamma_n + \beta T^2$, where γ_n is the Sommerfeld coefficient, and β is the Debye constant. The values of γ_n and β were obtained by fitting the normal-state data denoted by the solid red line in the inset of Fig. 3 and found to be $9.77(6) \text{ mJ mol}^{-1} \text{ K}^{-2}$ and $0.534(1) \text{ mJ mol}^{-1} \text{ K}^{-4}$, respectively. The Debye temperature (θ_D) is calculated using the expression

$$\theta_D = \left(\frac{12\pi^4 R N}{5\beta} \right)^{1/3}, \quad (6)$$

where R is the universal gas constant, and N is the number of atoms per formula unit. The obtained value of θ_D is calculated to be 221(1) K, which is higher than the θ_D obtained from resistivity measurements. The discrepancy in the θ_D values obtained from two different measurements is likely due to the different temperature ranges used in resistivity (10–300 K) and specific heat (10–15 K) measurements. Additionally, the resistivity model considers only the contribution of longitudinal phonons in electron-phonon scattering, while the specific heat model considers both transverse and longitudinal phonons. These differences in temperature range and model approximations have led to discrepancies in the extracted Debye temperature value. The deduced value of γ_n is larger than that of the parent $2H\text{-TaS}_2$ compound. Using the formula $\gamma_n = (\frac{\pi^2 k_B^2}{3}) D(E_F)$, we calculated the density of states (DOS) at the Fermi level to be 4.15(2) states $\text{eV}^{-1} \text{ f.u.}^{-1}$ for Li_xTaS_2 . Compared to $2H\text{-TaS}_2$ [38,39], the observed DOS near the Fermi level is higher in Li_xTaS_2 , which may be

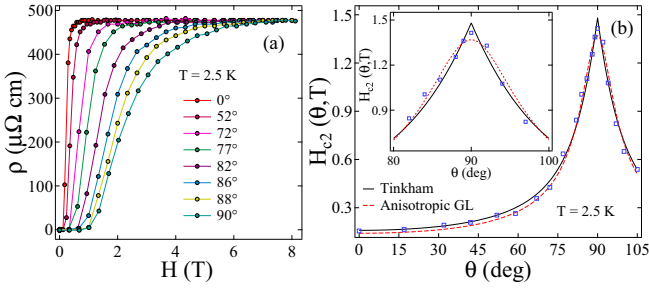


FIG. 4. (a) Field-dependent resistivity at $T = 2.5$ K and at different angles θ , where θ denotes the angle between the ab plane of the crystal and magnetic field direction. (b) Angular dependence of H_{c2} fitted with the 3D anisotropic GL (red) and the 2D Tinkham model (black). In the inset, an enlarged view of $H_{c2}(\theta)$ is shown within $\pm 10^\circ$ of $\theta = 90^\circ$.

related to the enhancement of the superconducting transition temperature compared to the parent $2H$ -TaS₂.

The strength of the electron-phonon interaction, λ_{e-ph} , can be estimated according to McMillan's theory [40] using the relation

$$\lambda_{e-ph} = \frac{1.04 + \mu^* \ln(\theta_D/1.45T_c)}{(1 - 0.62\mu^*) \ln(\theta_D/1.45T_c) - 1.04}, \quad (7)$$

where μ^* is taken to be 0.13 for transition metals, indicating a pseudopotential of effective electron repulsion. Thus, λ_{e-ph} is estimated to be 0.62, which manifests Li_xTaS₂ as a weakly coupled superconductor.

To investigate the symmetry of the superconducting gap, the electronic specific heat (C_{el}) is calculated using $C_{el}(T) = C(T) - \beta T^3$. The low-temperature electronic specific heat plot in Fig. 3 fits well with the s -wave model, as observed in Cu_xTiSe₂ [41]. According to this model, the entropy S for a single-gap BCS superconductor can be expressed as

$$S = -\frac{6\gamma_n}{\pi^2} \left(\frac{\Delta(0)}{k_B} \right) \int_0^\infty [f \ln f + (1-f) \ln(1-f)] dy, \quad (8)$$

where $f(\xi)$ is the Fermi function, defined as $f(\xi) = \{\exp[E(\xi)/k_B T] + 1\}^{-1}$, $E(\xi) = \sqrt{\xi^2 + \Delta^2(t)}$ is the excitation energy of the quasiparticles measured relative to the Fermi energy, $y = \xi/\Delta(0)$, $t = T/T_c$, and $\Delta(t) = \tanh\{1.82[1.018(1/t) - 1]^{0.51}\}$ is the temperature-dependent superconducting energy gap function. The temperature-dependent electronic specific heat can be calculated as $C_{el} = t \frac{dS}{dt}$. From the fit, it is found that the ratio of the superconducting gap $\Delta(0)/k_B T_c$ and the specific heat jump $\Delta C_{el}/\gamma_n T_c$ is approximately equal to 1.57 and 1.14, respectively. Both values are close to the BCS value (1.76 and 1.43) in the weak-coupling limit. However, further confirmation of the exact nature of the superconducting gap requires low-temperature measurements ($T < 0.2T_c$).

D. Angle-dependent magnetotransport measurement

To further explore the 2D superconducting properties, angle-dependent transport measurements of Li_xTaS₂ crystal were performed. The field-dependent resistivity at different angles at $T = 2.5$ K is presented in Fig. 4(a). The sample was

rotated from angle $\theta = 0^\circ$ ($H \parallel c$) to $\theta = 90^\circ$ ($H \perp c$), with the current always directed along the ab plane. The upper critical field, H_{c2} , was calculated at $\rho = 0.1\rho_n$. The angular dependence of H_{c2} is shown in Fig. 4(b) with a blue square symbol, which exhibits a cusplike variation with θ close to 90° .

The angular dependence of H_{c2} in anisotropic superconductors is typically explained by two theoretical models. For three-dimensional superconductivity, the angular dependence of H_{c2} can be represented in a simple ellipsoidal form according to the anisotropic GL model [42]:

$$\left(\frac{H_{c2}(\theta) \sin \theta}{H_{c2}^\perp} \right)^2 + \left(\frac{H_{c2}(\theta) \cos \theta}{H_{c2}^\parallel} \right)^2 = 1. \quad (9)$$

Meanwhile, for two-dimensional thin-film superconductors, Tinkham [43] proposed the following equation:

$$\left(\frac{H_{c2}(\theta) \sin \theta}{H_{c2}^\perp} \right)^2 + \left| \frac{H_{c2}(\theta) \cos \theta}{H_{c2}^\parallel} \right| = 1. \quad (10)$$

The superconductivity in a 2D regime can be modeled as superconducting layers separated by nonsuperconducting blocking layers. To determine the nature of superconductivity in Li_xTaS₂, the extracted H_{c2} values with angles were fitted using both the 2D Tinkham model and the 3D anisotropic GL model shown in Fig. 4(b). The data was more consistent with the 2D Tinkham model, indicating a quasi-2D nature of superconductivity in Li_xTaS₂.

E. Berezinskii-Kosterlitz-Thouless transition

The quasi-2D nature of Li_xTaS₂ is further supported by the measurement of temperature-dependent $V(I)$ characteristics, which reveal the BKT transition temperature. In systems approaching the 2D limit, strong spatial and temporal fluctuations can destroy phase coherence and superconductivity. However, BKT theory allows the phase transition to occur by establishing quasi-long-range correlations in the order parameter without breaking the symmetry [44,45]. While the observation of BKT transition in bulk layered crystals is rare, the $V(I)$ characteristics of Li_xTaS₂ manifest this transition, as shown in Fig. 5(a). At low temperatures, the $V-I$ characteristics become nonlinear due to the finite critical current and follow a power-law behavior given by

$$V \propto I^{\alpha(T)}, \quad \text{with } \alpha(T) = 1 + \pi J_s(T)/T, \quad (11)$$

where J_s is the superfluid density. Above T_c , the $V-I$ characteristics follow a general linear behavior corresponding to $\alpha = 1$. At the BKT transition, α increases to 3. By fitting the power law in Eq. (11), we have calculated the exponent values as a function of temperature, as shown in Fig. 5(b). We obtain $T_{BKT} = 2.9$ K, where $\alpha(T)$ reaches 3. The same α values were also obtained by plotting $d(\log V)/d(\log I)$ as a function of current, as shown in Fig. 5(c).

The quasi-2D behavior observed through the angular dependence of the upper critical field and the BKT transition suggests that intercalating Li atoms in $2H$ -TaS₂ weakens interlayer coupling and significantly changes electronic properties. In the monolayer limit of $2H$ -TaS₂, Ising SOC induced robust superconductivity against high magnetic fields [18]

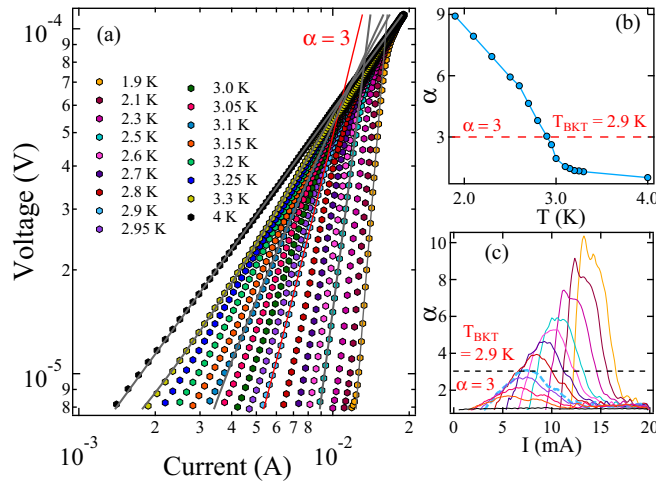


FIG. 5. (a) Temperature dependence of V - I curves at zero applied field to calculate BKT transition temperature. All solid gray lines indicate power-law fitting, and the red line indicates power-law fitting with $\alpha = 3$ corresponding to $T_{\text{BKT}} = 2.9$ K. (b) The exponent α values, calculated by the power-law fitting of different V - I isotherms. (c) α is also calculated by plotting $d(\log V)/d(\log I)(I) = \alpha$. The dashed line indicates $T_{\text{BKT}} = 2.9$ K corresponds to $\alpha = 3$.

has been observed, which is facilitated by the presence of heavy Ta atoms that contribute to a strong SOC. Our sample exhibited a high upper critical field that slightly exceeded the Pauli limit in the in-plane direction, prompting interest in investigating the source of the high H_{c2} in the bulk sample. Examining thickness-dependent superconductivity can also lead to exploring a more pronounced 2D nature and enhanced

SOC, which can lead to exotic Ising/FFLO type superconductivity and other quantum phenomena.

IV. CONCLUSION

We conducted transport, magnetization, and specific heat measurements on single crystals of Li-intercalated $2H$ -TaS₂ grown using the chemical vapor transport method. Our results demonstrate that bulk, anisotropic, weakly coupled s -wave superconductivity in Li _{x} TaS₂ where the upper critical field (H_{c2}) exceeds the Pauli limit. The angular dependence of the upper critical field (H_{c2}) conforms to the Tinkham model, denoting quasi-two-dimensional superconductivity. We also observed the BKT transition, affirming the quasi-two-dimensional nature of superconductivity. The breaking of the Pauli limit and the quasi-2D superconductivity suggest an unconventional pairing mechanism that requires additional low-temperature thickness dependence measurements for a better understanding. In addition, the easily cleavable nature of superconducting $2H$ -Li _{x} TaS₂ provides a unique opportunity to explore quantum phenomena and investigate intercalated 2D materials for novel quantum behavior.

ACKNOWLEDGMENTS

T.A. acknowledges the Department of Science and Technology (DST), Government of India, for support through the JRF fellowship under Award No. DST/INSPIRE/03/2021/002666. R.P.S. acknowledges Science and Engineering Research Board, Government of India, for Core Research Grant No. CRG/2019/001028.

- [1] Y. Saito, T. Nojima, and Y. Iwasa, Highly crystalline 2D superconductors, *Nat. Rev. Mater.* **2**, 16094 (2016).
- [2] A. W. Tsen, B. Hunt, Y. D. Kim, Z. J. Yuan, S. Jia, R. J. Cava, J. Hone, P. Kim, C. R. Dean, and A. N. Pasupathy, Nature of the quantum metal in a two-dimensional crystalline superconductor, *Nat. Phys.* **12**, 208 (2016).
- [3] Y. Xing, H.-M. Zhang, H.-L. Fu, H. Liu, Y. Sun, J.-P. Peng, F. Wang, X. Lin, X.-C. Ma, Q.-K. Xue, J. Wang, and X. C. Xie, Quantum Griffiths singularity of superconductor-metal transition in Ga thin films, *Science* **350**, 542 (2015).
- [4] Y. Xing, K. Zhao, P. Shan, F. Zheng, Y. Zhang, H. Fu, Y. Liu, M. Tian, C. Xi, H. Liu, J. Feng, X. Lin, S. Ji, X. Chen, Q.-K. Xue, and J. Wang, Ising superconductivity and quantum phase transition in macro-size monolayer NbSe₂, *Nano Lett.* **17**, 6802 (2017).
- [5] J. M. Lu, O. Zheliuk, I. Leermakers, N. F. Q. Yuan, U. Zeitler, K. T. Law, and J. T. Ye, Evidence for two-dimensional Ising superconductivity in gated MoS₂, *Science* **350**, 1353 (2015).
- [6] N. Reyren, S. Thiel, A. D. Caviglia, L. F. Kourkoutis, G. Hammerl, C. Richter, C. W. Schneider, T. Kopp, A.-S. Rüetschi, D. Jaccard, M. Gabay, D. A. Muller, J.-M. Triscone, and J. Mannhart, Superconducting interfaces between insulating oxides, *Science* **317**, 1196 (2007).
- [7] T. Soma, K. Yoshimatsu, K. Horiba, H. Kumigashira, and A. Ohtomo, Two-dimensional superconductivity in single-band correlated $2H$ -type NbO₂ layers, *Phys. Rev. B* **105**, 104504 (2022).
- [8] X. Hua, F. Meng, Z. Huang, Z. Li, S. Wang, B. Ge, Z. Xiang, and X. Chen, Tunable two-dimensional superconductivity and spin-orbit coupling at the EuO/KTaO₃(110) interface, *npj Quantum Mater.* **7**, 97 (2022).
- [9] H. Yang, S. W. Kim, M. Chhowalla, and Y. H. Lee, Structural and quantum-state phase transitions in van der Waals layered materials, *Nat. Phys.* **13**, 931 (2017).
- [10] Y. Saito, Y. Kasahara, J. Ye, Y. Iwasa, and T. Nojima, Metallic ground state in an ion-gated two-dimensional superconductor, *Science* **350**, 409 (2015).
- [11] A. Devarakonda, H. Inoue, S. Fang, C. Ozsoy-Keskinbora, T. Suzuki, M. Kriener, L. Fu, E. Kaxiras, D. C. Bell, and J. G. Checkelsky, Clean 2D superconductivity in a bulk van der Waals superlattice, *Science* **370**, 231 (2020).
- [12] H. Katzke, P. Tolédano, and W. Deppe, Phase transitions between polytypes and intralayer superstructures in transition metal dichalcogenides, *Phys. Rev. B* **69**, 134111 (2004).
- [13] W. Li, X. Qian, and J. Li, Phase transitions in 2D materials, *Nat. Rev. Mater.* **6**, 829 (2021).

- [14] S. Manzeli, D. Ovchinnikov, D. Pasquier, O. V. Yazyev, and A. Kis, 2D transition metal dichalcogenides, *Nat. Rev. Mater.* **2**, 17033 (2017).
- [15] A. H. Castro Neto, Charge Density Wave Superconductivity, and Anomalous Metallic Behavior in 2D Transition Metal Dichalcogenides, *Phys. Rev. Lett.* **86**, 4382 (2001).
- [16] T. Valla, A. V. Fedorov, P. D. Johnson, P.-A. Glans, C. McGuinness, K. E. Smith, E. Y. Andrei, and H. Berger, Quasiparticle Spectra, Charge-Density Waves, Superconductivity, and Electron-Phonon Coupling in 2H-NbSe₂, *Phys. Rev. Lett.* **92**, 086401 (2004).
- [17] X. Qian, J. Liu, L. Fu, and J. Li, Quantum spin Hall effect in two-dimensional transition metal dichalcogenides, *Science* **346**, 1344 (2014).
- [18] S. C. de la Barrera, M. R. Sinko, D. P. Gopalan, N. Sivadas, K. L. Seyler, K. Watanabe, T. Taniguchi, A. W. Tsen, X. Xu, D. Xiao, and B. M. Hunt, Tuning Ising superconductivity with layer and spin-orbit coupling in two-dimensional transition-metal dichalcogenides, *Nat. Commun.* **9**, 1427 (2018).
- [19] J. G. Guo, X. Chen, X. Y. Jia, Q. H. Zhang, N. Liu, H. C. Lei, Y. Li, L. Gu, S. F. Jin, and X. L. Chen, Quasi-two-dimensional superconductivity from dimerization of atomically ordered AuTe₂Se_{4/3} cubes, *Nat. Commun.* **8**, 871 (2017).
- [20] L. K. Ma, M. Z. Shi, B. L. Kang, K. L. Peng, F. B. Meng, C. S. Zhu, J. H. Cui, Z. L. Sun, D. H. Ma, H. H. Wang, B. Lei, T. Wu, and X. H. Chen, Quasi-two-dimensional superconductivity in SnSe₂ via organic ion intercalation, *Phys. Rev. Mater.* **4**, 124803 (2020).
- [21] X. Yang, T. Yu, C. Xu, J. Wang, W. Hu, Z. Xu, T. Wang, C. Zhang, Z. Ren, Z.-a. Xu, M. Hirayama, R. Arita, and X. Lin, Anisotropic superconductivity in the topological crystalline metal Pb_{1/3}TaS₂ with multiple Dirac fermions, *Phys. Rev. B* **104**, 035157 (2021).
- [22] I. Guillamón, H. Suderow, J. G. Rodrigo, S. Vieira, P. Rodière, L. Cario, E. Navarro-Moratalla, C. Martí-Gastaldo, and E. Coronado, Chiral charge order in the superconductor 2H-TaS₂, *New J. Phys.* **13**, 103020 (2011).
- [23] C. Patra, T. Agarwal, R. R. Chaudhari, and R. P. Singh, Two-dimensional multigap superconductivity in bulk 2H-TaSeS, *Phys. Rev. B* **106**, 134515 (2022).
- [24] R. V. Coleman, G. K. Eiserman, S. J. Hillenius, A. T. Mitchell, and J. L. Vicent, Dimensional crossover in the superconducting intercalated layer compound 2H-TaS₂, *Phys. Rev. B* **27**, 125 (1983).
- [25] D. Johnston and B. Keelan, Superconductivity and magnetism of M_x(H₂O)_yTaS₂ layered cointercalation compounds, *Solid State Commun.* **52**, 631 (1984).
- [26] H. Liu, S. Huangfu, X. Zhang, H. Lin, and A. Schilling, Superconductivity and charge density wave formation in lithium-intercalated 2H-TaS₂, *Phys. Rev. B* **104**, 064511 (2021).
- [27] J. P. Tidman, O. Singh, A. E. Curzon, and R. F. Frindt, The phase transition in 2H-TaS₂ at 75 K, *Philos. Mag.* **30**, 1191 (1974).
- [28] A. H. Wilson, The electrical conductivity of the transition metals, *Proc. R. Soc. London A* **167**, 580 (1938).
- [29] J. Bardeen, L. N. Cooper, and J. R. Schrieffer, Theory of superconductivity, *Phys. Rev.* **108**, 1175 (1957).
- [30] R. C. Morris and R. V. Coleman, Anisotropic superconductivity in layer compounds, *Phys. Rev. B* **7**, 991 (1973).
- [31] L. Fang, Y. Wang, P. Y. Zou, L. Tang, Z. Xu, H. Chen, C. Dong, L. Shan, and H. H. Wen, Fabrication and superconductivity of Na_xTaS₂ crystals, *Phys. Rev. B* **72**, 014534 (2005).
- [32] X. Zhu, Y. Sun, S. Zhang, J. Wang, L. Zou, L. E. DeLong, X. Zhu, X. Luo, B. Wang, G. Li, Z. Yang, and W. Song, Anisotropic intermediate coupling superconductivity in Cu_{0.03}TaS₂, *J. Phys.: Condens. Matter* **21**, 145701 (2009).
- [33] L. Li, X. Zhu, Y. Sun, H. Lei, B. Wang, S. Zhang, X. Zhu, Z. Yang, and W. Song, Superconductivity of Ni-doping 2H-TaS₂, *Phys. C (Amsterdam, Neth.)* **470**, 313 (2010).
- [34] S. Ilić, J. S. Meyer, and M. Houzet, Enhancement of the Upper Critical Field in Disordered Transition Metal Dichalcogenide Monolayers, *Phys. Rev. Lett.* **119**, 117001 (2017).
- [35] Y. Cao, J. M. Park, K. Watanabe, T. Taniguchi, and P. Jarillo-Herrero, Pauli-limit violation and re-entrant superconductivity in moiré graphene, *Nature (London)* **595**, 526 (2021).
- [36] R. A. Klemm, A. Luther, and M. R. Beasley, Theory of the upper critical field in layered superconductors, *Phys. Rev. B* **12**, 877 (1975).
- [37] Y. Li, Z. Wu, J. Zhou, K. Bu, C. Xu, L. Qiao, M. Li, H. Bai, J. Ma, Q. Tao, C. Cao, Y. Yin, and Z.-A. Xu, Enhanced anisotropic superconductivity in the topological nodal-line semimetal In₃TaS₂, *Phys. Rev. B* **102**, 224503 (2020).
- [38] F. J. D. Salvo, R. Schwall, T. H. Geballe, F. R. Gamble, and J. H. Osiecki, Superconductivity in Layered Compounds with Variable Interlayer Spacings, *Phys. Rev. Lett.* **27**, 310 (1971).
- [39] P. Garoche, P. Manuel, J. J. Veyssié, and P. Molinié, Dynamic measurements of the low-temperature specific heat of 2H-TaS₂ single crystals in magnetic fields, *J. Low Temp. Phys.* **30**, 323 (1978).
- [40] W. McMillan, Transition temperature of strong-coupled superconductors, *Phys. Rev.* **167**, 331 (1968).
- [41] S. Y. Li, G. Wu, X. H. Chen, and L. Taillefer, Single-Gap *s*-Wave Superconductivity near the Charge-Density-Wave Quantum Critical Point in Cu_xTiSe₂, *Phys. Rev. Lett.* **99**, 107001 (2007).
- [42] M. Tinkham, *Introduction to Superconductivity* (Courier Corporation, North Chelmsford, MA, 2004).
- [43] M. Tinkham, Effect of fluxoid quantization on transitions of superconducting films, *Phys. Rev.* **129**, 2413 (1963).
- [44] J. M. Kosterlitz and D. J. Thouless, Ordering, metastability and phase transitions in two-dimensional systems, *J. Phys. C: Solid State Phys.* **6**, 1181 (1973).
- [45] P. Minnhagen, Kosterlitz-Thouless transition for a two-dimensional superconductor: Magnetic-field dependence from a Coulomb-gas analogy, *Phys. Rev. B* **23**, 5745 (1981).